



Contents lists available at ScienceDirect

Smart Health

journal homepage: [www.elsevier.com/locate/smhl](http://www.elsevier.com/locate/smhl)

# Smartphone-based Human Hemoglobin Level Measurement Analyzing Pixel Intensity of a Fingertip Video on Different Color Spaces

Md Kamrul Hasan<sup>a,\*</sup>, Munirul Haque<sup>b</sup>, Nazmus Sakib<sup>a</sup>, Richard Love<sup>a</sup>,  
Sheikh I. Ahamed<sup>a</sup>

<sup>a</sup> Mathematics, Statistics and Computer Science Department, Marquette University, USA

<sup>b</sup> Regenstrief Center for Healthcare Engineering (RCHE), Purdue University, USA

## ARTICLE INFO

### Keywords:

Non-invasive hemoglobin  
Smartphone-based hemoglobin measurement  
Color-space conversion  
Image-based hemoglobin level prediction  
PLS-based hemoglobin measurement

## ABSTRACT

Non-invasive methods in the assessment of health parameters are important for various kinds of patient, but only few expensive and inconvenient solutions are available. Investigations of non-invasive methods beginning with simple red-green-blue (RGB) imaging extending to hyper-spectral camera-based image have encountered portability, usability, and reliability issues. This paper presents a smartphone-based non-invasive hemoglobin level prediction model that addresses portability, accuracy and ease-of-use problems by taking advantage of the built-in high-resolution camera, significant computation ability, storage, and communication facility of current smartphones. In this research work, RGB information of a 10-second fingertip videos is used to convert into different color spaces including hue (H), saturation (S), value (V), lightness (L), a, b (a and b for the color dimensions) and gray (g). Later, features are extracted from all the combinations of ten different colors and applied to a Partial Least Squares (PLS) algorithm. We have evaluated the best color combination to generate a prediction model with the data collected from American and Bangladeshi patients. Our model with a specific pixel color combination achieves a reliable accuracy.

## 1. Introduction

There is increasing interest and research on non-invasive methods in assessment of health parameters. First, patients prefer non-invasive medical tests. Second, frequent invasive tests are difficult for many patients and are not applicable to patients such as premature infants, older individuals, hemoglobinopathy patients and patients needing frequent assessments. Third, invasive testing is time-expensive. Finally, the set-up costs for invasive testing are high for small healthcare-provider businesses. To better address the needs of patients and caregivers, the development low-cost non-invasive, point of care (P-O-C) tools is desirable.

Smartphone approaches to these assessment challenges can potentially address expense and mobility. In addition to having significant computational power, storage, and communication capability, smartphones are ubiquitous globally. These features offer the possibility of low-cost and widespread application of smartphone hemoglobin assessment tools. Since smartphones have demonstrated usefulness as mHealth P-O-C tools for activity detection (Kawsar, Hasan, Love, & Ahamed, 2015; Kawsar et al., 2016),

\* Corresponding author.

E-mail addresses: [mdkamrul.hasan@marquette.edu](mailto:mdkamrul.hasan@marquette.edu) (M.K. Hasan), [mhaque@purdue.edu](mailto:mhaque@purdue.edu) (M. Haque), [nazmus.sakib@marquette.edu](mailto:nazmus.sakib@marquette.edu) (N. Sakib), [Richard.Love@marquette.edu](mailto:Richard.Love@marquette.edu) (R. Love), [sheikh.ahamed@marquette.edu](mailto:sheikh.ahamed@marquette.edu) (S.I. Ahamed).

URL: <http://www.mscc.mu.edu/~mhasan02/> (M.K. Hasan).


<https://doi.org/10.1016/j.smhl.2017.11.003>

Received 1 May 2017; Received in revised form 7 November 2017; Accepted 8 November 2017

2352-6483/© 2017 Elsevier Inc. All rights reserved.

**Table 1**

Prediction of physiological data using video image analysis based on different color spaces.

Ref.	Objectives	Findings	Color Space
[9]	To measure cardiac pulse using facial video.	Green pixel gave $r=0.95$ .	●
[10]	To measure arterial blood oxygen level.	Good accuracy founds despite motion and noise.	●
[11]	To quantify arterial blood oxygen (SpO <sub>2</sub> ) level.	Satisfactory result.	● ●
[12]	To measure hemoglobin concentration using conjunctival erythema index (EI).	Sensitivity of 93% and 57% and specificity of 78% and 83%.	● ●
[13]	To eliminate physiological data.	Mean Absolute Error (MAE) of the heart rate increased from 0.254 bpm to 17bpm.	● ● ●
[14]	To observe bio-signals from video.	MAE=9.89 bpm, 1.6% SPO <sub>2</sub> , 19.93 mmHg (systolic bpm).	● ● ●
[15]	To calculate heart rate using RGB, monochrome and a thermal camera.	RGB + thermal camera gave satisfactory output.	● ● ● ● ●
[16]	To measure hemoglobin level noninvasively.	Sensitivity and precision of 85.7% and 76.5%.	● ● ● ● ●
Current report	To determine Hb level non-invasively: 10-second-fingertip video, extract RGB of 100 images frames, convert RGB to hue (H), saturation (S), value (V), Lightness (L), a, b (a and b for the color dimensions) and gray (g) color space.	Generate histogram values, average for each video and apply PLS algorithm. $R^2 = 95\%$ for specific combination of feature matrix input.	● ● ● ● ● 

cancer care (Love et al., 2016), pain level identification (Hasan, Ahsan, Ahamed, Love & Salim, 2016), eESAS (Haque et al., 2015) and point-of-care diagnostics, we have chosen to explore use of this tool for hemoglobin level measurement. In our approach, we collect only patient fingertip videos with the flashlight on, while following the recommended video capturing protocols. We have employed no additional sensors or equipment. After video recording, blood samples are collected in the usual invasive manner immediately from the patient for gold standard hemoglobin assessment. Investigators have reported different levels of performance of their non-invasive tool measurements based on various color pixel selections from videos shown in Table 1. Extending these approaches involves assessing specific color pixel and color combinations data. The basic flowchart of smartphone-based hemoglobin level prediction model is presented in Fig. 1.

In a previous report, we have presented an RGB pixel analysis and showed correlations with low and high levels of hemoglobin (Hasan et al., 2017; Ahsan et al., 2017). We also converted the RGB pixels in to Hue, Saturation and Value (HSV) with additional fingertip videos. The result of the HSV-based pixel analysis (Hasan, Sakib, Field, Love & Ahamed, 2017) gave us direction for the different color analysis that we report here. In the current communication, we report:

1. A novel fingertip and smartphone camera setup to capture a ten-second video for hemoglobin level identification.
2. A fingertip video processing system that can produce histogram values as well as input feature matrix in different color space.
3. An extensive analysis on sickle cell patient- (who received blood transfusion) fingertip video data to understand how the frequency of different color pixel intensity is increased for the same finger with lower and higher level of hemoglobin.
4. A demonstration of how the combination of different color (feature) matrix of a fingertip video can increase the accuracy level of a prediction model.

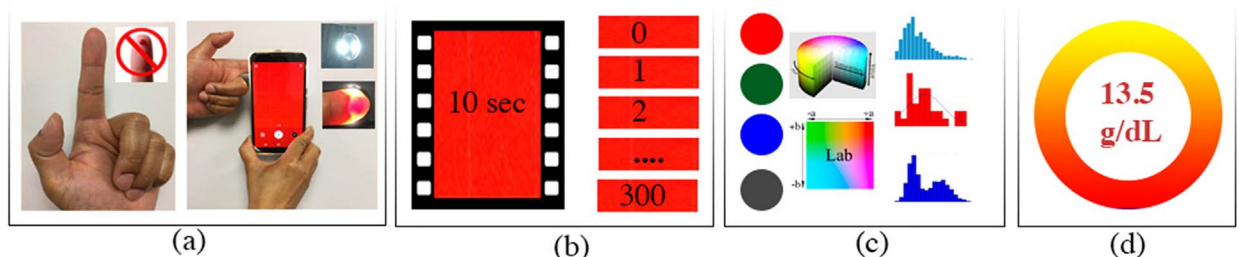


**Fig. 1.** Smartphone-based hemoglobin level prediction model a) the index-finger is put on the smartphone camera with the camera ash on b) a 10 s fingertip video is taken generating 300 frames (30fps) c) each frames red, green, blue pixel intensities are converted into hue, saturation, value, gray and Lab color space.

To the best of our knowledge, this manuscript is the first to report on non-invasive hemoglobin level prediction using a smart-phone without any additional accessories, with satisfactory precision, low cost, and easy usability. Additionally, this report is different in proposing a hemoglobin prediction model based on fingertip video data under color space variation.

## 2. Related work

Non-invasive tools for assessments of hemoglobin (Hb), glucose, heart rate, and bio-signals measurement have been described. Based on contact-lens-amperometric (Yao, Shum, Cowan, Lähdesmäki, & Parviz, 2011; Yao et al., 2012), NovioSense (Thomas, Nicole, Lähdesmäki, & Parviz, 2012), ultrasound (Vashist, 2012; Tierney et al., 2001), and tears (Yan et al., 2011), non-invasive glucose measurement systems have been investigated. These non-invasive systems are less than ideal because of high cost, limited accuracy, and difficulty in use. Physiological data assessment tools for cardiac pulse extraction (Wedekind et al., 2017), physiological data elimination (Chen.), bio-signals measurement (Lee, Seo, Yang, Park, & Hong, 2016) and thermal imaging (Garbey, Sun, Merla, & Pavlidis, 2007; Fei & Pavlidis, 2010) for heart (HR) and respiration rate (RR) monitoring (Poh, McDu, & Picard, 2010; Poh, McDu, & Picard, 2011; Lewandowska, Ruminski, Kocajko, & Nowak, 2011; Shao et al., 2014), and blood volume pulse (Wei, Tian, Wang, Ebrahimi, & Huang, 2012; Belkin & Niyogi, 2003; Monkaresi, Calvo, & Yan, 2014) have been reported. In most cases, image information has been used, where red, green and blue pixels of the image are used to create the input features. Among these three colors, red and green pixels play more prominent roles in reported

results.

More recently, diversified non-invasive methods for measuring hemoglobin concentration have been proposed. Among these, the majority have involved optical measurement of blood in the fingertip. To determine the ratio of hemoglobin to water in blood plasma, one team developed a finger probe consisting of 6 LEDs that cover multiple wavelengths of 630, 660, 680, 770, 880 and 1300 nm (Abdallah et al., 2010; Alam, 2011). Subsequently, Kraitl, Timm, Lewis, and Ewald (2010) demonstrated similar

results using a three LED (670, 810, 1300 nm) finger probe, in a study of 41 individuals. Based on this work Timm et al. (2015) developed a device named OxyTrue Hb. Subsequently Masimo developed an expensive commercially available system that incorporates 7 LEDs and uses a proprietary algorithm (Macknet, Allard, Applegate, & Rook, 2010). These non-invasive systems present multiple problems. The visible and infrared light spectrum is sensed using different LED lights that complicate the data collection. Further these approaches are expensive and the devices are complex in computational and operational dimensions. Hyperspectral camera and spectrometers-based non-invasive hemoglobin level prediction (Yuan et al., 2015; Paul et al., 2015; Singh, Dubey, Sonker, & Chaudhary, 2015; Ardin et al., 2015) tools manifest much precision, but are also expensive. For example, Wang et al. presented a smartphone-based application named as HemaApp (Wang et al., 2016). They analyzed fingertip video data captured under different lighting sources. They used incandescent and LED lights to enlighten the fingertip and analyzed RGB pixels from the captured video. In 31 subjects (from 6–77 years of age), and they demonstrated a sensitivity of 85.7% and an accuracy of 76.5%.

In the above-mentioned approaches, the proposed solutions have multifaceted problems like use of multiple wavelengths of LED, commercially expensive, and external attachments. In our approach, we do not use any surface hardware. We collect only patient fingertip videos with the flashlight on. Blood samples are collected immediately from the patient for gold standard hemoglobin assessment. We assess the specific color pixel and color combinations.

data to get the smartphone-based hemoglobin level prediction model without any significant cost.

## 3. Theory

In healthy adults, the hemoglobin (Hb) concentration in blood is 150 g/liter. Hb carries nearly 65 times more oxygen than plasma in blood. Oxygenated blood is more red in color than deoxygenated blood since blood absorbs the frequencies of visible light but reflects red due to hemoglobin. Since hemoglobin absorbs some lights and reflects other lights, we can predict the concentration of Hb in blood vessels with an appropriate light absorbance calculation. Hemoglobin absorbs green light strongly. Since green light is not able to penetrate deeper into tissues, green light does not have strong significance in hemoglobin concentration measurement because Hb is a deeper tissue parameter. On the other hand, red light is transparent to skin melanin. As a result, skin color does not affect the red-light transmission through it. Different colored pixel-based research has been developed to assess Hb non-invasively (Hasan, Sakib, Field, & Ahamed, 2017). Examples of different physiological data measurement research using video images and various color spaces in their prediction models are shown in Table 1. Because of these findings, the idea of exploring different color spaces has been taken and applied in the research reported here.

### 3.1. Use of color-space in reported research

Video-based physiological information measurement assessments have been done, in most of which facial and fingertip video images are considered for bio-signal prediction. In biomarker prediction-based research, videos are captured using smartphone, regular, thermal and hyper-spectral cameras. A smartphone camera is less expensive and is more user-friendly. Since the video-based process is non-invasive, researchers have explored image-based analysis for the measurement of hemoglobin level, glucose level, heart rate, blood pressure, blood oxygen saturation, and gesture recognition. The video capturing methodologies are different in each approach. In general, facial video is captured in most reported studies. In some investigations, the illumination is changed while capturing video or fingertip video is employed.

In video-based regression analysis, the color space is critical. Red, green, blue, hue, saturation, value, L, a, b, gray colors have

been studied. Chen et al. used the intensity of red, green and blue colors from facial videos (Chen,). They computed L-level Laplacian pyramids for each color channel without affecting the original visual appearance. Wedekind et al. captured video in RGB mode and chose green wavelength for cardiac pulse rate selection (Wedekind et al., 2017).

Single green pixel intensity has been used in automated cardiac pulse measurements (Poh et al., 2010), arterial blood oxygenation level calculation (Chen,), and to detect poor physical condition (Yoshizawa et al., 2016). Although RGB color space was used initially in those studies, the authors achieved better accuracy later using the video analysis with green pixel data only. Gupta et al. used magenta and thermal color channels with RGB color space for HR measurement (Gupta, McDu, & Raskar, 2016). They analyzed their results with different combinations of input channels and found that a red, green and thermal color combination gave the best results. Carni et al. found significant predictive value for a combination of red and green pixel data for blood oxygenation level evaluation (Carni, Grimaldi, Sciammarella, Lamonaca, & Spagnuolo, 2016). Wang used two different wavelength of LED lights: white and incandescent, for video data capturing. They used average intensity of RGB color space for hemoglobin level prediction (Wang et al., 2016). Drawing from the chromatic analyses of video, we extracted RGB intensities from fingertip video image and converted the RGB intensities to HSV, Lab and gray color space.

### 3.2. Histogram values of an image

A color histogram- a bar-graph-illustration of each pixel intensity of an image- represents the total color description of a particular image (Tournier et al., 2017). We can generate color histograms for a particular color from different color space, such as RGB (commonly used), HSV, and Lab (Kawakami,). From a statistical standpoint, a color histogram focuses on the distribution of Different colors, regardless of their spatial location. The major drawback of histogram data is that its representation is color-dependent for a particularly considered object, ignoring its shape and texture. Hence, it is possible for the color histograms for two images with different object content to be identical if they share the same color information. Despite these issues, color histogram is considered as a simple and visually strong indicator of a picture in the domain of computer vision and image processing. In the reported work, we represent the histogram using 256 bins for each image. Fig. 2 shows histograms for two different mages of a subject having hemoglobin levels of 7.5 g/dL and 10.3 g/dL.

### 3.3. Relationship between fingertip image and hemoglobin level

We have investigated the hemoglobin level concerning a fingertip image of a severe sickle cell patient in (Hasan et al., 2017). This patient had the Hb level 7.2 g/dL before the blood transfusion and 10.5 g/dL after the blood transfusion. The RGB, as well as respective masked and histogram image of these both periods, are presented in Fig. 3. In the histogram, we can observe that the RGB color intensity of fingertip image for the lower level of hemoglobin has more frequency than that of the higher level of Hb. Using image mask, we found that the mask image has higher black pixel for the lower level of Hb than that of a higher level of Hb. Further details on this research are published in (Hasan et al., 2017).

### 3.4. Color space conversion

Although different color spaces manifest unique information from a particular image, it is possible to convert the color information from one color space to another with several derived equations. Here, for the reported work, the essential conversion equations are presented for converting from RGB to HSV, Lab, and Gray color spaces.

#### 3.4.1. RGB to HSV color space

The information of the RGB Color space can be converted to that of the HSV color space by the following equation sets (Table 2).

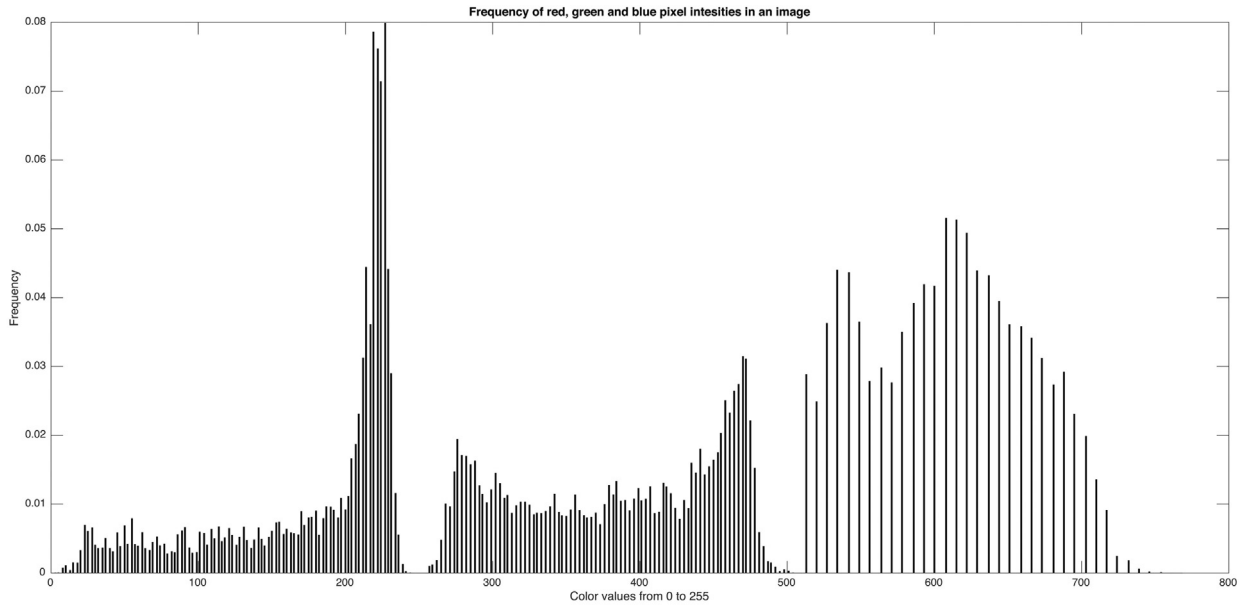
#### 3.4.2. RGB to Lab color space

In the case of Lab color space, conversion of the RGB information first to the XYZ color space information where Y means luminance, Z is equivalent to blue, and X is orthogonal to luminance and non-negative. Then, from XYZ, we can convert the RGB color space information to Lab Color space data (Ford & Roberts, 1998).

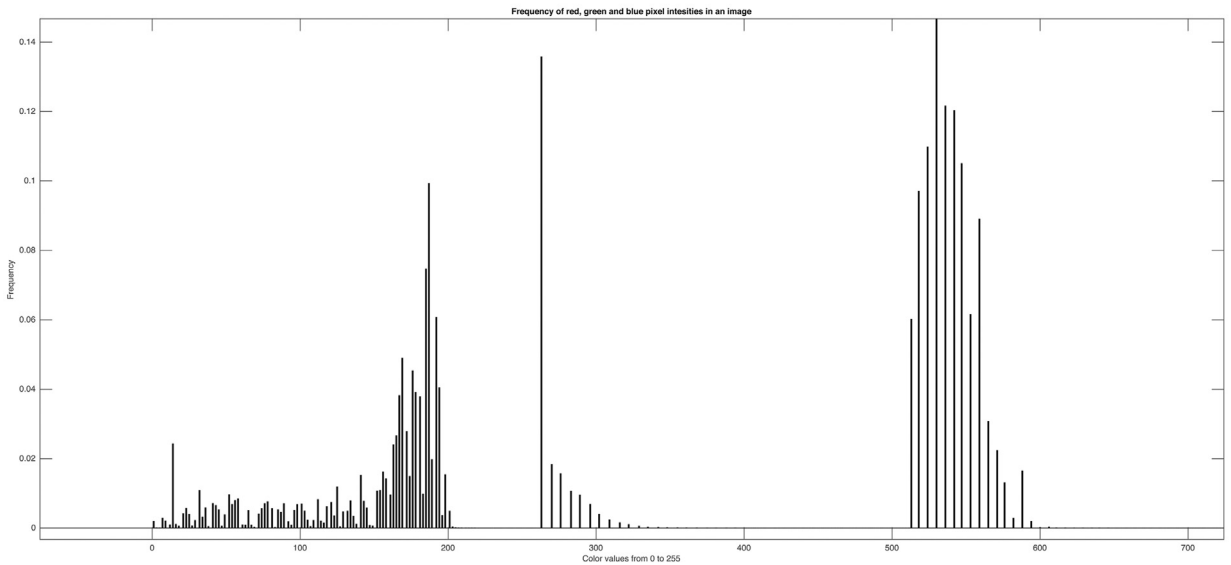
#### 3.4.3. RGB to gray color space

In general, there are three conversion techniques commonly practiced changing RGB color space information to gray scale information. The first is the lightness method. In this technique, we obtain the arithmetical mean of the most prominent and the least prominent colors. It is written as  $(\max(R, G, B) + \min(R, G, B)) / 2$ . The second is the average method. It only takes the average of the values:  $(R + G + B) / 3$ . The most sophisticated is the luminosity method. While it also averages the values, it takes a weighted mean to account for human perception. Here, we are more sensitive to the green color information than that of the other colors. Hence, the green is weighted more in the following equation. The luminosity formula is  $0.21 R + 0.72 G + 0.07 B$  (Cook,).

For each video, we first took the image frames and converted these frames to RGB color space. Then, the HSV, Lab and gray color spaces were also generated from RGB using the above noted methods. We generated histogram values for each color space and applied a PLS algorithm to build a final hemoglobin prediction model.



(a) Hb 7.5 g/dL.



(b) Hb 10.3 g/dL.

**Fig. 2.** Histogram of a fingertip image. Same subject with severe anemia (a) and post-blood transfusion (b).

#### 4. Methodology

We used Google Nexus 4.0 (LG) smartphones for data collection in two countries: Bangladesh and USA.

##### 4.1. Patient information

We collected fingertip videos from two different groups of patients. The first group (Group-A), consists of five patients with sickle cell hemoglobinopathy. These patients were under care at The Blood Center of Wisconsin (BCW), USA. The second group of patients were recruited among normal adults from seen in an AmaderGram Clinic in Khulna, Bangladesh. Patient consent, as well as IRB approval, were obtained in both USA and Bangladesh for the collection of data from both populations.

We considered these patients invasive blood Hb results as the observation gold standard. Since the sickle cell patients had lower than normal levels of hemoglobin, they were often treated with blood transfusions. We collected fingertip videos and Hb standard test

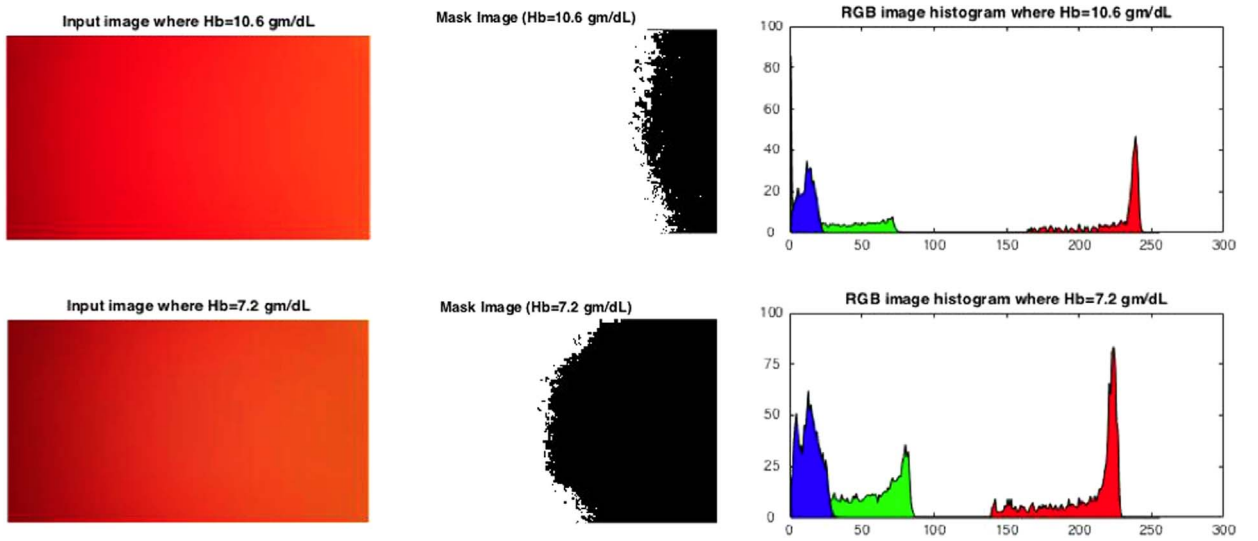


Fig. 3. The masked image and RGB variations of two fingertip images are shown for the same person when the subject is with different level of hemoglobin.

Table 2  
RGB to HSV Conversion.

$$\begin{aligned}
 R &= \frac{R}{255}, G = \frac{G}{255}, B = \frac{B}{255} \\
 C_{max} &= \text{Max}(R, G, B) \\
 C_{min} &= \text{Min}(R, G, B) \\
 \Delta &= C_{max} - C_{min} \\
 V &= C_{max}
 \end{aligned}
 \quad
 S = \begin{cases} 0 & \text{if } C_{max}=0 \\ \frac{\Delta}{C_{max}} & \text{if } C_{max} \neq 0 \end{cases}$$

$$V = \begin{cases} 0^0 & \Delta = 0 \\ 60^0 \times \left( \frac{G-B}{\Delta} \times \text{mod}6 \right) & C_{max}=R \\ 60^0 \times \left( \frac{B-R}{\Delta} \times \text{mod}6 \right) & C_{max}=G \\ 60^0 \times \left( \frac{R-G}{\Delta} \times \text{mod}6 \right) & C_{max}=B \end{cases}$$

data for these patients before and after their blood transfusions. In both cases, the video was recorded immediately before blood sample collection. During the data collection on the sickle cell patients we had two individuals with significant hand and finger tremulousness while capturing the fingertip video. Because of this, for all these 5 sickle cell patients, we recorded three fingertip videos for each measurement, to try and minimize the noise introduced. Thus, we obtained fifteen videos associated with five Hb level reports before blood transfusion and 15 post transfusion. Each fingertip video was treated as an individual observation, so we had a total of thirty observations from this patient-group. The second patient group (Group-B), was of 75 volunteer healthy subjects with age range from 20 years to 56 years. One subject's hemoglobin report was lost so we had blood samples and fingertip videos from 74 patients of whom fifty-five were female and nineteen males. We collected one fingertip video and one gold standard Hb measurement for each subject. We kept separate these both Group-A and B data set in our analysis for the following reasons:

- i) Group-A people have sickle cell problem and very low level of hemoglobin.
- ii) Subjects in the Group-B were healthy and with higher hemoglobin level.
- iii) Population size were not equal.
- iv) The Group-A provided data in western setup where the Group-B gave sample in rural area of Bangladesh.
- v) The data analysts recommend not to mix different population data to reduce the variance in the input matrix though bias in data can result from here.

#### 4.2. Methods of data capture

The comprehensive fingertip video and feature extraction process is presented in Fig. 1. Once the video was captured from the index finger of a subject, the second step was to generate frames and RGB pixel intensities for each frame. Finally, the color space conversions were made.

Feature extractions process from a fingertip video is presented in Fig. 4. Once the video is captured from the index finger of a subject, the second step is to generate frames and RGB pixel intensities for each frame. Finally, the color space conversion is happened in the 3rd step as shown in Fig. 4.



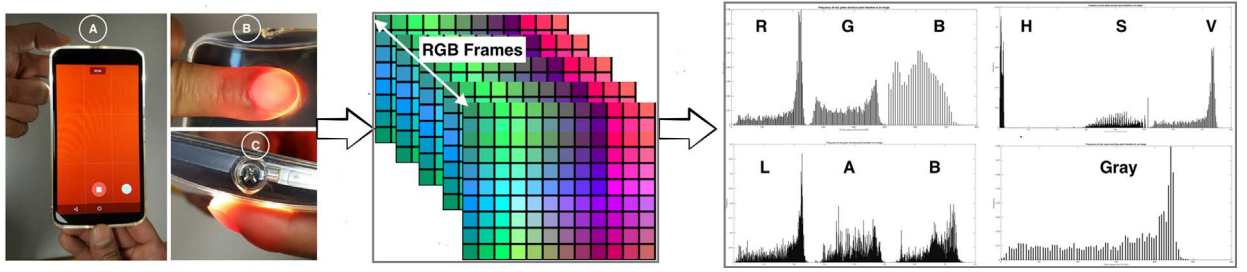


Fig. 4. Fingertip video was recorded with the flash light on. One hundred frames were created and RGB pixels were extracted from each frame. Finally, RGB pixels were converted into HSV, Lab and gray color spaces.

#### 4.2.1. Video capture

Research coordinators followed the following protocol in recording the fingertip videos.

- The video was made before taking the invasive gold standard blood sample.
- The index finger was chosen.
- The smartphone camera was covered to exclude any ambient light as shown in Fig. 5.
- The ash mechanism was turned on as shown in Fig. 4.
- A 10-second video was recorded with the index finger inmobly touching the camera lens.

#### 4.3. Feature extraction

Smart phones videos record 30 frames per second (fps) that result in 300 frames for a 10-second video. Before color intensity analysis, we checked each fingertip video playing one by one. We observed that for most of the first 50 frames there was noise (black/very dark areas) for 30% of the videos and often also in the last section of the frames sequences. Because of these findings we chose to use frames 101–200 to for our feature matrices.

##### 4.3.1. Feature matrix

We created one feature vector per fingertip video. A feature vector is a combination of one or more single color feature vectors. The single-color feature vector was created using pixel intensities from 100 frames. First, we created a histogram for each color of pixel intensities with 256 number of the bin for a frame. Since the pixel intensities are from 0 to 255, we got the frequency of each color pixel intensity from the respective histogram. We generated 100 histogram values of each color for a single video. Finally, we averaged these 100 histogram values and stored them as single-color feature vectors. For example, the red pixel has intensity values from 0 to 255. We observed how many times each value between 0 and 255 appeared in a histogram when we took histogram values of red pixel of each frame. Since RGB color space of each image frame can be converted to HSV, Lab, and gray color space, we generated a feature vector for these individual color data. Here, the dimension of each single-color feature vector is  $1 \times 256$ . We considered ten different colors: red (R), green (G), blue (B), hue (H), saturation (S), value (V), lightness (L), a (color channel), b (color channel), and gray (g). If we combined two different color feature vectors, then the dimension of the feature vector will be  $1 \times 512$ . So, we could generate a feature vector of maximum dimension  $1 \times 2560$  for a video. Again, we produced a feature matrix with the greatest dimension  $30 \times 2560$  for 30 videos of group A patients and  $74 \times 2560$  for 74 observations of group B patients.

##### 4.3.2. Feature generation steps

For all observations in group A and B data, the step-by-step feature extraction process was as follows:



Fig. 5. Index finger covered the camera and flash light completely.

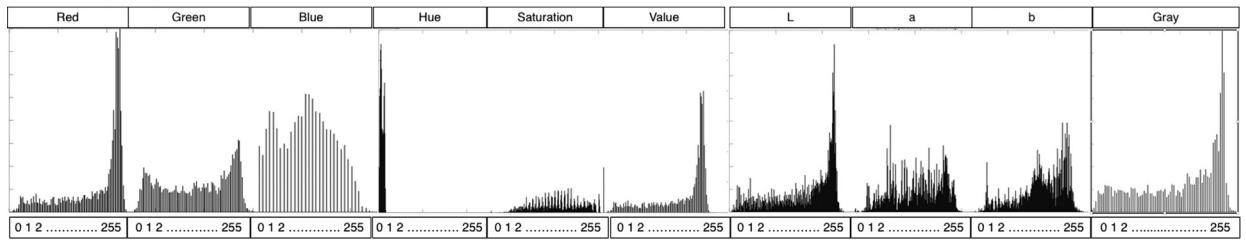


Fig. 6. The features of a video are generated by R, G, B, H, S, V, L, a, b, g color.

**Repeat steps 1 and 2 for data extraction from each video.**

Step 1: Extract the red, green, and blue (RGB) pixel intensities for each image frame.

Then convert RGB color space into.

1(a) Hue, saturation, value (HSV).

1(b) Lab and.

1(c) Gray (g) color space.

Step 2: Generate 100 histogram values of R, G, B, H, S, V, L, a, b, g color intensity (0–255) with 256 number of bins for 100 frames of a video and make average of each respective color frequency. We average 100 histogram value of different color frequency. Each average histogram value of R, G, B, H, S, V, L, a, b, and g is named as respective feature vector. Juxtaposition of all ten averaged feature vectors are shown in Fig. 6.

Step 3: **Feature matrix generation:** Let we want to consider only red (R) color pixel data of all videos as features. In this case, the dimension of R feature matrix will be  $30 \times 256$  for BCW and  $74 \times 256$  for AmaderGram data. If we add another color such as green (G) with R, then the feature matrix will be based on the juxtaposition of R and G. In this case, the dimension of the feature matrix increases to  $30 \times 512$  for BCW and  $74 \times 512$  for AmaderGram video. The size of the feature matrix changed based on the number of different color combination used. We consider 1023 number of different combinations using R, G, B, H, S, V, L, a, b and g color feature vectors in both dataset.

Step 4: We name the input feature matrix as X (later mentioned as predictor matrix X). The clinical hemoglobin levels stored in Y matrix (called response matrix Y later). Input feature matrix differ in size based on the number of color combination, but the response matrix Y (gold standard Hb values) is the size of 301 for BCW and 741 for AmaderGram.

Step 5: We standardize each input matrix before data analysis. In this case, each column of X are centered to have mean 0 and scaled to have standard deviation 1.

Step 6: We apply partial least squares (PLS) algorithm on each combination of feature matrix generated by BCW and AmaderGram data. We use 10-fold cross validation in PLS method. PLS algorithm produces prediction model based on the number of PLS components. We start with two PLS components and increased later to see how accuracy level improved for BCW video data. We choose 10 PLS components initially for AmaderGram video data and increase the number of PLS component to observe the change in performance. We take maximum 5 and 25 number of PLS components for BCW and AmaderGram fingertip video data respectively.

Based on the steps discussed above, we applied PLS algorithm with 10-fold cross validation on 1023 number of input feature matrix for both BCW and AmaderGram data. Each feature matrix of BCW was run for PLS components of 2, 4, and 5. Again, 10, 12, 15, 17, 20, 22 and 25 number PLS components applied on 1023 feature matrix of AmaderGram video data. The generated results of 1023 feature matrix for each PLS components sorted.

in descending order. We presented the top five coefficient of determination ( $R^2$ ) for each PLS components in tabular form and shown in the results section.

## 5. Results

In our previous research (Ahsan et al., 2017), we analyzed fingertip video data using regression and classification. In (Ahsan et al., 2017), we extract only RGB data from video image. We used individual RGB feature values and multivariate linear regression and we calculated the correlation coefficients. In the classification method, we use Decision Tree algorithms, SVM, and naive Bayes methods. Here we took the average values of data sets recorded before and after the blood transfusion.

From these values, we identified the differences and calculated the relationships with respect to the hemoglobin values. Previously we used multivariate linear regression and we applied singular value decomposition (SVD) to the data set. We found significant correlation coefficient but not clinically accepted. Here we also analyzed the confusion matrices and the ROC curves. Further, we used two classification algorithms: J48 method and ADTree.

Partial Least Squares Regression (PLSR) and Principal Components Regression (PCR) are modern tools for data analysis when we have a lot of features. The example in (Documentation, The mathworks, 2017) shows how PLSR and PCR behave on the Near Infrared Spectra analysis (Kalivas, 1997). Here, we observe that which regression tool is useful between PLSR and PCR. We know that PLSR and PCR model a response variable when we have a large number of predictor variables. PLSR and.

PCR build components as the linear combinations of the original predictor variables. PCR constructs component without considering the response variable, but PLSR considers the response variable. As a result, PLSR often provides better models than PCR to



**Table 3**

PLS algorithm applied on multiple color feature matrix of Group A patients for different PLS components.

(a) PLS component = 2			(b) PLS component = 3		
SL	Color	R <sup>2</sup>	SL	Color	R <sup>2</sup>
1	RSg	0.65574	1	RGSVLg	0.87353
2	SVg	0.65574	2	RGSVLag	0.87307
3	RBSg	0.65491	3	RGSVLabg	0.87231
4	BSVg	0.65491	4	RGSVLbg	0.86904
5	RBSLg	0.65113	5	RGSVabg	0.86896

fit the response variable with less number of components.

### 5.1. Group A

Because of the smaller data size for this group, we applied two PLS components initially. Later, we raise the number of PLS component up to 5 adding one PLS component each time to evaluate the influence of PLS components. We generated the prediction model with two PLS components with 10-fold cross validation. This prediction model has given maximum R<sup>2</sup> for color a (a is from color space Lab) when we consider a color feature matrix. In Table 7a, we can see that other colors except b are also close to the accuracy achieved by color a. The lowest R<sup>2</sup> value is observed for b that was from the same color space Lab.

We observed better results with two PLS components when we combined several feature matrices. The combination of feature matrix R, S and g generated the best R<sup>2</sup>. In the top five combinations, R and S features are found. Three PLS components gave better outcome for the feature matrix combination of R, G, S, V, L, and g. The other combinations also showed nearly 87% accuracy. Table 4a and b present R<sup>2</sup> for PLS component 4 and 5 where top five results are also very close to each other.

### 5.2. Group-B patients

Since this data set was bigger than that of group A, we started with 10 PLS components and 10-fold cross validation for regression analysis. We choose 10, 12, 15, 17, 20, 22 and 25 PLS components to assess for changes in accuracy of the prediction model. We applied feature matrices of size from 74256 to 74 × 2560 for each number of PLS components. Note that a single-color feature matrix has the dimension of 74256 and we have generated 1023 combination of input feature matrix where the maximum dimension of input feature matrix is 74 × 2560. We sort out the R<sup>2</sup> values for each feature matrix applied with 10, 12, 15, and 17 PLS components and present the top five R<sup>2</sup> values in Table 5a and b.

In the same way, we considered 20, 22 and 25 PLS components to apply the PLS algorithm with 10-fold cross validation on 1023 combination of input feature matrix. R<sup>2</sup> value for these PLS components, varied from 0.95 to 0.98 for various input feature models. Table 6a and b present the top five R<sup>2</sup> values generated with 20, 22 and 25 PLS components for the group-B data.

The noticeable thing is that we did not find optimum R<sup>2</sup> values for any single color applying PLS on both data sets (Table 7). We observe that the most and best accurate R<sup>2</sup> for PLS components of 15 and 17 (Table 5a). Feature matrices with the combination of R, B, H, a, and b or B, H, V, a, and b generate 71% and 79% accurate model predictions with PLS 10 and 12 components respectively. The other combinations show better predictions with lower numbers of color mixing. For example, a feature matrix made of R, B, a and b showed significant prediction accuracy.

We obtained higher accuracy by increasing the number of PLS components. In Table 5b for example, higher levels of prediction accuracy are observed for PLS components 15 and 17. With these higher levels, the previous.

combination of feature (RBHb or BHVab) matrix don't show. Here, the input feature matrix that is made of the combination of R, B, S, V, a, and b gives us 87% and 95% prediction model for group-B data. A previous color.

combination is observed in this Table 5b with prediction accuracy similar to R, B, S, V, a, and b.

When we evaluated more PLS components with different combination of feature matrices, we found that combination of R, B, S, L, a, b, and g feature matrices gave us R<sup>2</sup> = 0.95. A similar result was also seen with the combination of feature matrix B, S, V, L, a, b,

**Table 4**

Mixed color feature matrix of Group-A patients is run by PLS algorithm for different PLS components.

(a) PLS component = 4			(b) PLS component = 5		
SL	Color	R <sup>2</sup>	SL	Color	R <sup>2</sup>
1	RGSVLag	0.95933	1	RGHVLabg	0.98718
2	RGHSVLag	0.95925	2	RGVLag	0.98582
3	RGSVLabg	0.95745	3	RGVLabg	0.98577
4	RGSVLg	0.95583	4	RGHVLag	0.98575
5	RGSL	0.95512	5	GVLabg	0.98565

**Table 5**

Mixed color feature matrices of group-B patients is run by PLS algorithm for different PLS components.

(a) R <sup>2</sup> for PLS components = 10 and 12				(b) R <sup>2</sup> for PLS components = 15 and 17			
SL	Color	10	12	SL	Color	15	17
1	RBHab	0.7097	0.7902	1	RBSVab	0.8743	0.924
2	BHVab	0.7097	0.7902	2	RBHsa	0.8708	0.9078
3	RBab	0.6999	0.7727	3	BHSVa	0.8708	0.9078
4	BVab	0.6999	0.7727	4	RHag	0.8683	0.9025
5	RBHSag	0.6996	0.7436	5	HVag	0.8683	0.9025

**Table 6**

Mixed color feature matrices of group-B patients is run by PLS algorithm for the PLS components = 20, 22 and 25.

(a) R <sup>2</sup> for PLS components= 20			(b) R <sup>2</sup> for PLS components= 22 and 25			
SL	Color	20	SL	Color	22	25
1	RBSLabg	0.9522	1	RGBHSLa	0.9698	0.9881
2	BSVLabg	0.9522	2	GBHSVLa	0.9698	0.9881
3	RBHSLabg	0.9512	3	RGBSLa	0.9695	0.9881
4	BHSVLabg	0.9512	4	GBSVLa	0.9695	0.9881
5	RBSLag	0.9509	5	RGBHSLab	0.9693	0.9867

**Table 7**

Single color feature matrix of Groups-A and B is run by PLS algorithm for PLS components 2 and 10 respectively.

(a) PLS Component = 2 (BCW)			(b) PLS Component = 10 (AmaderGram)		
SL	Color	R <sup>2</sup>	SL	Color	R <sup>2</sup>
1	a	0.56884	1	R	0.5369
2	G	0.53311	2	V	0.5369
3	L	0.53165	3	L	0.5305
4	R	0.52347	4	g	0.4823
5	V	0.52347	5	B	0.4752
6	g	0.44683	6	S	0.4547
7	H	0.44487	7	a	0.4366
8	B	0.42154	8	G	0.4221
9	S	0.40295	9	b	0.3397
10	b	0.16942	10	H	0.2291

and g, (Table 6a). We observed R<sup>2</sup> values of 0.97, 0.99 when the PLS components were 22 and 25 respectively for the feature matrix combination of R, G, B, H, S, L, and a or G, B, H, S, V, L, and a (a is from Lab color space) (Table 6b).

## 6. Discussion

Multiple different schemes have been used to analyze finger camera video data for a physiological data prediction models shown (Table 1). Some investigators have used only R, G, and B colors initially, and selected a single-color following data analysis. Other investigators have looked at multiple color spaces (Carni et al., 2016; Gupta et al., 2016; Wang et al., 2016) (Table 1). For hemoglobin assessments, red pixels have been commonly used. Hemoglobin absorbs green light and reflects red light. For this reason, hemoglobin concentration affects tissue color (Setaro & Sparavigna, 2002). So, green pixel absorbance information is an important for video-based hemoglobin level assessment. In this report, we have gone beyond single color or combination of multiple color space investigation to explicitly identify which color or combination of colors are critical to an accurate model.

We discover the relationship between hemoglobin level and frequency of image pixel intensity analyzing blood transfusion data collected from BCW. We construct input feature matrix for 30 observations where the input data grid is built using the combination of ten color feature information. Fig. 7 shows the full input feature matrix of BCW data combining all color information. In this data set, the lowest level of hemoglobin is 2.6 g/dL, and highest value of that is 11.6 g/dL. The change in frequency of different color space is observed significantly if we deliberate histogram values of features matrix related to the lower and higher level Hb. Lower peaks manifest lower Hb level where higher peaks elucidate higher level of hemoglobin as shown in Fig. 7. We investigated the relationship between hemoglobin level and frequency of image pixel intensity, analyzing finger video images from anemic sickle cell hemoglobinopathy patients (Group-A) subjected to blood transfusion. We construct input feature matrices for 30 observations where the input data grid was built using the combination of ten different color features. Fig. 7 shows the full input feature matrix of these data

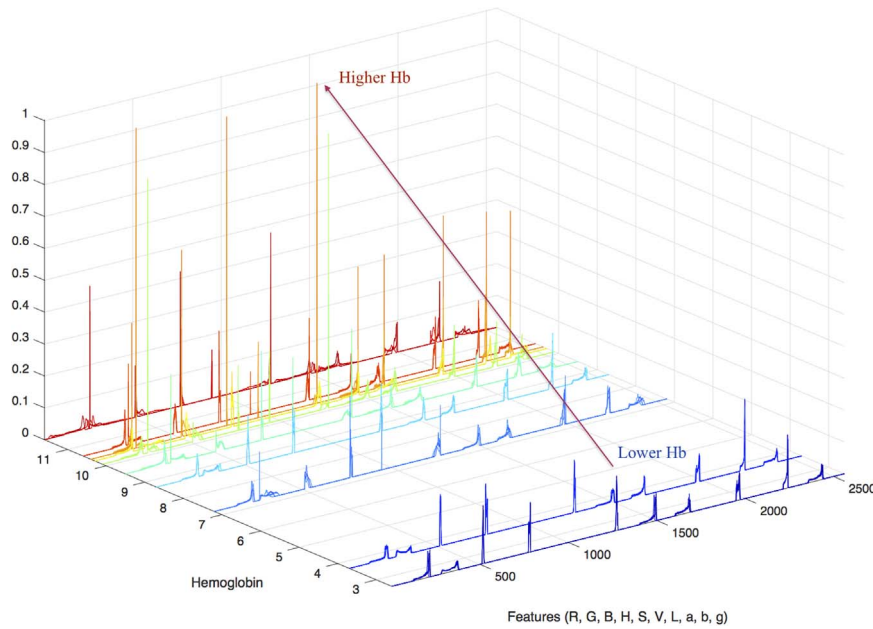


Fig. 7. The frequency of image pixel intensity changes with higher levels of hemoglobin.

combining all color information. In this data set, the lowest level of hemoglobin is 2.6 and highest value is 11.6 g/dL. The change in frequency of different color space is observed significantly if we look at the histogram values of features matrix related to the lower and higher level Hb. Lower peaks manifest lower Hb levels where higher peaks show higher levels of hemoglobin (Fig. 7). These initial forays into predictor matrix development using various color combination were then used for the model creation for a second normal patient (Group-B) data set. Table 7 represents the model accuracy for initial PLS components and single-color input feature data for both group A and B data sets.

In both cases, accuracy of the model is pretty close and every single color makes a meaningful contribution to prediction model development. Combinations of multiple color features reveal the most important findings (Table 3 and Table 4). The  $R^2$  values are similar for each PLS components value (Table 3a and b). R, G, S, V, L and g are frequently observed in the color combination here. R, G, S, and L is the lowest number of combination found for 4 PLS components that built a 95% accurate PLS model for Group-A data. Figs. 8 and 9 show the regression lines and residuals for PLS model of Group-A data. In the context of personalization, we can think about this prediction model. Since five patients provided two different fingertip videos with two different levels of Hb, our prediction model might be applied to build a personalized point-of-care (P-O-C) tool for such patients.

Feature matrices shown in Fig. 7 and improved model accuracies presented in Table 3a and b support the conclusion that combinations of different color features improve the performance of machine learning algorithms. Using the same technique for the second normal patient Group-B data set, Tables 5a, b, 6a and b show high  $R^2$  values for various PLS component numbers. A fixed color

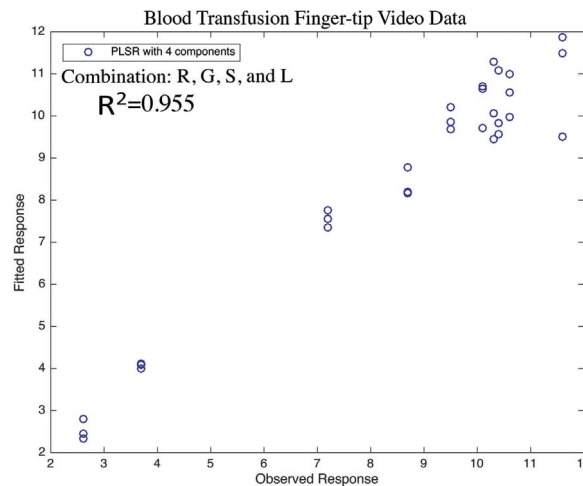


Fig. 8. PLS regression with 4 components (BCW).

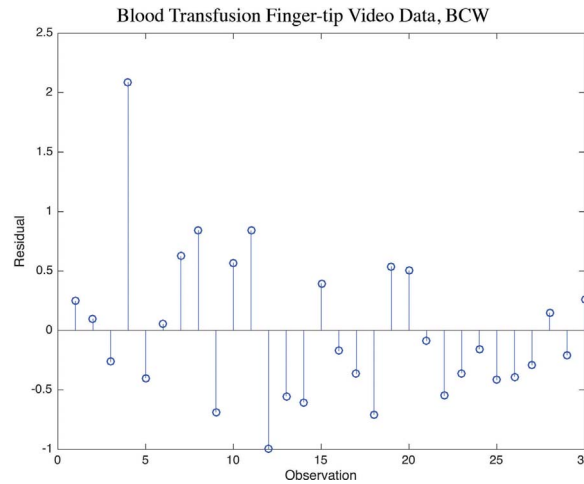


Fig. 9. Residuals generated by PLS regression (BCW).

combination does not provide continuous performance improvement with increases in the number of PLS components. R, B, S, L, a, and g provides 95% of accuracy with minimum numbers of combination. Here, R, G, B, S and L frequently appears in the combination of input feature matrices where the  $R^2$  values are higher. We found remarkable changes in  $R^2$  values with increasing the number of PLS components. The model performance improves through 20 PLS components. Above this number of components, the improvement rate slows down. The slow improvement signifies that growing PLS numbers overt the Hb prediction model. We present the improvement of  $R^2$  in Tables 8 and 9 for both group-A and group-B respectively. In Table 9, the minimum difference between two consecutive  $R^2$  value is seen after selecting 20 PLS components. The regression line and residuals for Group B video data with 20 PLS components are presented.

in Figs. 10 and 11.

The PLS weights are the linear combinations of the input variables of the feature matrix. PLS weights are used to define the PLS components. PLS weights tell us about how much each component in the PLSR depends on the original variables. It also gives us the direction (Documentation, The mathworks, 2017). Different image pixels are used here as the feature of each observation. Based on the feature combination, we have seen various results while selecting a different number.

of PLS components. We observe  $R^2 = 95\%$  for 30 observations of the group-A where RGSL color combination are used shown in Table 4a. We found the similar quantity of  $R^2$  shown in Table 6a for 74 subjects' fingertip observations where the RBSLabg color combination is used for group-B. Here 20 PLS components are used since the data size is bigger than the group-A dataset. So, based on the data size and location, we observe that the PLS.

components are different and also the features sets vary.

Among the different combination of all features, we observe that red (R) pixel is mostly available in all of the combination. But, only red pixel cannot describe the whole relevant features to the physiological characteristics of fingertip. For this reason, we have presented this novel idea to make different combination of color pixels and apply to generate a robust regression model using PLS.

## Conclusions

Based on smartphone finger-tip video data, a noninvasive hemoglobin prediction model is proposed that predicts Hb concentration with 95% accuracy. The fingertip video is analyzed based on a different feature (color) matrix to get the minimum number of PLS components. To keep the number of feature matrices at a minimum requiring less computation and yet yield an optimal result, we created a histogram value as well as feature matrices in different.

Table 8

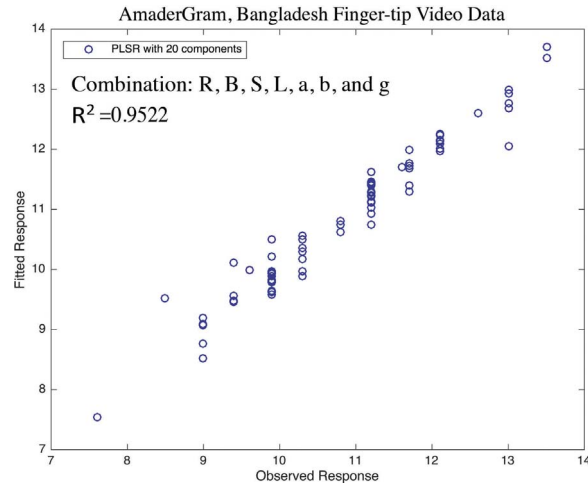
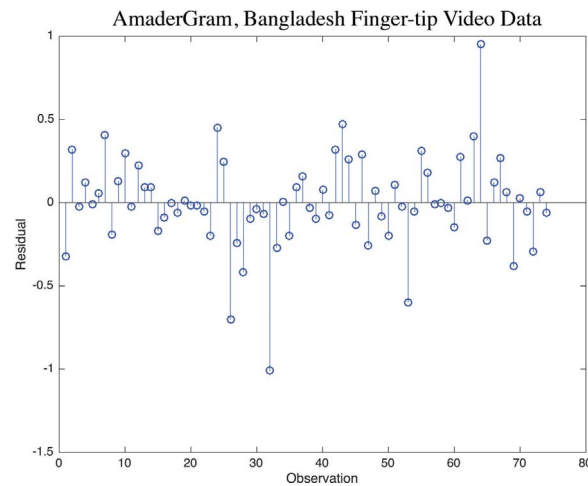
Best accuracy with optimum number of color and PLS components for Group-A data.

SL	Color mixture	PLS comp	$R^2$ value	Accuracy
1	RSg	2	0.65574	66%
2	SVg	2	0.65574	66%
3	RGSVLg	3	0.87353	87%
4	RGSVLag	3	0.87307	87%
5	RGSVLag	4	0.95933	96%
6	RGHSVLag	4	0.95925	96%
7	RGHVLagb	5	0.98718	99%
8	RGVLag	5	0.98582	99%

**Table 9**

Best accuracy with optimum number of color and PLS components for Group-B data.

SL	Color mixture	PLS comp	R <sup>2</sup> value	Accuracy
1	RBHab	10	0.7097	71%
2	BHVab	10	0.7097	71%
3	RBHab	12	0.7902	79%
4	BHVab	12	0.7902	79%
5	RBSVab	15	0.8743	87%
6	RBSVab	17	0.924	92%
7	RBSLabg	20	0.9522	95%
8	BSVLabg	20	0.9522	95%

**Fig. 10.** PLS regression using 20 components (AmaderGram).**Fig. 11.** Residuals generated by PLS (AmaderGram).

color space. We studied two different patient data sets. We expect to further expand this work to study how other color space, skin thickness, and melanin tuning aspects the prediction model. We also plan to apply PCA, Decision Tree algorithms, SVM, J48 method, ADTree and naive Bayes methods for hemoglobin level classification in future.

### Acknowledgements

This project is partially supported by a grant from IBCRF, USA, a grant from Medical College of Wisconsin (01070-74779) (MCW), USA and Ubicomp lab, Marquette University, USA. The authors are grateful to Dr. Hargarten SW of the Emergency Medicine Department, MCW, Dr. Joshua Field of Blood Center of Wisconsin, MCW and the supporting colleagues and staffs who helped us for

the data collection from the blood research center.

## References

- Kawsar, F., Hasan M., Love R., & Ahamed S. (2015). A novel activity detection system using plantar pressure sensors and smartphone, In Computer Software and Applications Conference (COMPSAC) IEEE 39th Annual, 1 (pp. 44–49). IEEE.
- Kawsar, F., Hasan M., Tanvir Roushan, Ahamed S., Chu W., & Love R. (2016). Activity Detection Using Time-Delay Embedding, In Multi-modal Sensor System. In *International Conference on Smart Homes and Health Telematics* (pp. 489–499). Springer, Cham.
- Love, R. R., Ferdousy, T., Paudel, B. D., Nahar, S., Dowla, R., Adibuzzaman, M., Ahsan, G. M. T., Uddin, M., Salim, R., & Ahamed, S. I. (2016). Symptom levels in care-seeking Bangladeshi and Nepalese adults with advanced cancer. *Journal of Global Oncology* (JGO004119).
- Hasan, Md. Kamrul, Ahsan, Golam Mushih Tanimul, Ahamed, Sheikh Iqbal, Love, Rechard, & Salim, Reza (2016). Pain level detection from facial image captured by smartphone. *Journal of Information Processing*, 24(4), 598–608.
- Haque, M. M., Kawsar, F., Adibuzzaman, M., Uddin, M. M., Ahamed, S. I., Love, R., Hasan, R., Dowla, R., Ferdousy, T., & Salim, R. (2015). e-esas: Evolution of a participatory design-based solution for breast cancer (bc) patients in rural bangladesh. *Personal and Ubiquitous Computing*, 19(2), 395–413.
- Hasan M.K., Sakib N., Love J.F., SW H., R R., Ahamed S.I. (2017). Rgb pixel analysis of fingertip video image captured from sickle cell patient with low and high level of hemoglobin, In Proceedings of the 8th IEEE Annual Ubiquitous Computing, Electronics Mobile Communication Conference Columbia University, New York City, NY, USA, 19–21 October 2017, IEEE.
- Ahsan G.M., Gani M.O., Hasan M.K., Ahamed S.I., Chu W., Adibuzzaman M., Field J. (2017). A novel real-time non-invasive hemoglobin level detection using video images from smartphone camera, In Computer Software and Applications Conference (COMPSAC), 2017 IEEE 41st Annual, 1, IEEE (pp. 967–972).
- Hasan M. K., Sakib N., Field J., Love R. R., Ahamed S. I. (2017). A novel technique of noninvasive hemoglobin level measurement using hsv value of fingertip image, In 2017 IEEE In Proceedings of the 41st Annual Computer Software and Applications Conference (COMPSAC), IEEE (pp. 221–229).
- Poh, M.-Z., McDu, D. J., & Picard, R. W. (2010). Non-contact, automated cardiac pulse measurements using video imaging and blind source separation. *Optics express*, 18(10), 10762–10774.
- Carni D., Grimaldi D., Sciammarella P., Lamonaca F., Spagnuolo V. (2016). Setting-up of ppg scaling factors for spo2% evaluation by smartphone, In Medical Measurements and Applications (MeMeA), 2016 IEEE International Symposium on, IEEE (pp. 1-spo5).
- Chen W., Picard R. W. Eliminating physiological information from facial videos.
- Lee H. -H., Seo E. -J., Yang J. -S., Park S. -M., Hong K. -S. (2016). Video-based bio-signal measurements for a mobile healthcare system, In Proceedings of the 10th International Conference on Ubiquitous Information Management and Communication, ACM (p. 92).
- Gupta O., McDu D., Raskar R. (2016). Real-time physiological measurement and visualization using a synchronized multi-camera system, In Proceedings of the IEEE Conference on Computer Vision and Pattern Recognition Workshops (pp. 46–53).
- Wang E. J., Li W., Hawkins D., Gernsheimer T., Norby-Slycord C. Patel S. N. (2016). Hemaapp: noninvasive blood screening of hemoglobin using smartphone cameras, In Proceedings of the 2016 ACM International Joint Conference on Pervasive and Ubiquitous Computing, ACM (pp. 593–604).
- Yao, H., Shum, A. J., Cowan, M., Lähdesmäki, I., & Parviz, B. A. (2011). A contact lens with embedded sensor for monitoring tear glucose level. *Biosensors and Bioelectronics*, 26(7), 3290–3296.
- Yao, H., Liao, Y., Lingley, A. R., Afanasiev, A., Lähdesmäki, I., Otis, B. P., & Parviz, B. A. (2012). A contact lens with integrated telecommunication circuit and sensors for wireless and continuous tear glucose monitoring. *Journal of Micromechanics and Microengineering*, 22(7), 075007.
- Thomas, Nicole, Lähdesmäki, Ilkka, & Parviz, Babak A. (2012). A contact lens with an integrated lactate sensor. *Sensors and Actuators B: Chemical*, 162.1, 128–134.
- Vashist, S. K. (2012). Non-invasive glucose monitoring technology in diabetes management: A review. *Analytica chimica acta*, 750, 16–27.
- Tierney, M. J., Tamada, J. A., Potts, R. O., Jovanovic, L., Garg, S., Team, C. R., et al. (2001). Clinical evaluation of the glucoWatch® biographer: A continual, non-invasive glucose monitor for patients with diabetes. *Biosensors and Bioelectronics*, 16(9), 621–629.
- Yan, Q., Peng, B., Su, G., Cohan, B. E., Major, T. C., & Meyerho, M. E. (2011). Measurement of tear glucose levels with amperometric glucose biosensor/capillary tube configuration. *Analytical chemistry*, 83(21), 8341–8346.
- Wedekind, D., Trumpp, A., Gaetjen, F., Rasche, S., Matschke, K., Malberg, H., & Zaunseder, S. (2017). Assessment of blind source separation techniques for video-based cardiac pulse extraction. *Journal of Biomedical Optics*, 22(3) (035002-035002).
- Garbey, M., Sun, N., Merla, A., & Pavlidis, I. (2007). Contact-free measurement of cardiac pulse based on the analysis of thermal imagery. *IEEE Transactions on Biomedical Engineering*, 54(8), 1418–1426.
- Fei, J., & Pavlidis, I. (2010). Thermistor at a distance: Unobtrusive measurement of breathing. *IEEE Transactions on Biomedical Engineering*, 57(4), 988–998.
- Poh, M.-Z., McDu, D. J., & Picard, R. W. (2011). Advancements in noncontact, multiparameter physiological measurements using a webcam. *IEEE Transactions on Biomedical Engineering*, 58(1), 7–11.
- Lewandowska M., Ruminski J., Kociejko T., Nowak J. (2011). Measuring pulse rate with a webcamera noncontact method for evaluating cardiac activity, In Computer Science and Information Systems (FedCSIS), 2011 Federated Conference on, IEEE (pp. 405–410).
- Shao, D., Yang, Y., Liu, C., Tsow, F., Yu, H., & Tao, N. (2014). Noncontact monitoring breathing pattern, exhalation flow rate and pulse transit time. *IEEE Transactions on Biomedical Engineering*, 61(11), 2760–2767.
- Wei L., Tian Y., Wang Y., Ebrahimi T., Huang T. (2012). Automatic webcam-based human heart rate measurements using laplacian eigenmap, In Asian Conference on Computer Vision, Springer (pp. 281–292).
- Belkin, M., & Niyogi, P. (2003). Laplacian eigenmaps for dimensionality reduction and data representation. *Neural computation*, 15(6), 1373–1396.
- Monkarese, H., Calvo, R. A., & Yan, H. (2014). A machine learning approach to improve contactless heart rate monitoring using a webcam. *IEEE Journal of Biomedical and Health Informatics*, 18(4), 1153–1160.
- O. Abdallah O. Natsheh M. Alam K. A. Qananwah Q. Al Nabulsi A. Bolz A. (2010). Concentrations of hemoglobin fractions calculation using modied lambert-beer law and solving of an ill-posed system of equations, in: SPIE Photonics Europe, International Society for Optics and Photonics (pp. 771511–771511).
- Alam K. A. (2011). Fuzzy logic hemoglobin sensors, (Ph.D. thesis), Karlsruhe Inst. für Technologie, Diss., 2011.
- Kraitl J. Timm U. Lewis E. Ewald H. (2010). Optical sensor technology for a noninvasive continuous monitoring of blood components, in: BiOS, International Society for Optics and Photonics (pp. 757209–757209).
- Timm U. Gewiss H. Kraitl J. Stuepmann K. Hinz M. Koball S. Ewald H. (2015). Novel multi wavelength sensor concept to detect total hemoglobin concentration, methemoglobin and oxygen saturation, in: SPIE BiOS, International Society for Optics and Photonics (pp. 93320J–93320J).
- Macknet, M. R., Allard, M., Applegate, R. L., Rook, J., et al. (2010). The accuracy of noninvasive and continuous total hemoglobin measurement by pulse co-oximetry in human subjects undergoing hemodilution. *Anesthesia Analgesia*, 111(6), 1424–1426.
- Yuan, X., Tsai, T.-H., Zhu, R., Llull, P., Brady, D., & Carin, L. (2015). Compressive hyperspectral imaging with side information. *IEEE Journal of Selected Topics in Signal Processing*, 9(6), 964–976.
- Paul, D. W., Ghassemi, P., Ramella-Roman, J. C., Prindeze, N. J., Moatt, L. T., Alkhalil, A., & Shupp, J. W. (2015). Noninvasive imaging technologies for cutaneous wound assessment: A review. *Wound Repair and Regeneration*, 23(2), 149–162.
- Singh, A., Dubey, A., Sonker, A., & Chaudhary, R. (2015). Evaluation of various methods of point-of-care testing of haemoglobin concentration in blood donors. *Blood Transfusion*, 13(2), 233.
- Ardin, Sergey, Störmer, Melanie, Radojska, Stela, Oustianskaia, Larissa, Hahn, Moritz, & Gathof, Birgit S. (2015). Comparison of three noninvasive methods for hemoglobin screening of blood donors. *Transfusion*, 55(2), 379–387.
- Hasan M.K., Sakib N., Field, R R., Ahamed S.I. (2017). Analyzing the existing noninvasive hemoglobin measurement techniques, In Proceedings of the 8th IEEE Annual Ubiquitous Computing, Electronics Mobile Communication Conference Columbia University, New York City, NY, USA, 19 – 21 October 2017, IEEE.
- Yoshizawa M., Sugita N., Abe M., Tanaka A., Obara K., Yamauchi T., Homma N., Yambe T. (2016). Blood perfusion display based on video pulse wave, In Engineering



- in Medicine and Biology Society (EMBC), 2016 IEEE In Proceedings of the 38th Annual International Conference of the, IEEE (pp. 4763–4767).
- Tournier, C., de Lavergne, M. D., van de Velde, F., Stieger, M., Salles, C., & Bertrand, D. (2017). Investigation of oral gels breakdown using image analysis. *Food Hydrocolloids*, 63, 67–76.
- Kawakami Y., Hattori T., Imai Y., Ando K., Horikawa Y., Rajapakse R.J., Histogram matching based on gaussian distribution using variance estimation-comparing between curvature computation and regression analysis.
- Ford, A., & Roberts, A. (1998). *Colour space conversions*. 1998, London: Westminster University1–31.
- Cook J., Three algorithms for converting color to grayscale, The Endeavour.
- Documentation M. (2017), The mathworks.
- Kalivas, J. H. (1997). Two data sets of near infrared spectra. *Chemometrics and Intelligent Laboratory Systems*, 37(2), 255–259.
- Setaro, M., & Sparavigna, A. (2002). Quantification of erythema using digital camera and computer-based colour image analysis: A multicentre study. *Skin Research and Technology*, 8(2), 84–88.

## Further reading

- van Gastel M., Stuijk S., de Haan G. New principle for measuring arterial blood oxygenation, enabling motion-robust remote monitoring, Scientific Reports 6.
- Collings, S., Thompson, O., Hirst, E., Goossens, L., George, A., & Weinkove, R. (2016). Non-invasive detection of anaemia using digital photographs of the conjunctiva. *PloS one*, 11(4), e0153286.